The Upper-Oceanic Response to Overflows: A Mechanism for the Azores Current

SHINICHIRO KIDA*

Massachusetts Institute of Technology/Woods Hole Oceanographic Institution Joint Program, Woods Hole, Massachusetts

JAMES F. PRICE AND JIAYAN YANG

Woods Hole Oceanographic Institution, Woods Hole, Massachusetts

(Manuscript received 20 December 2006, in final form 31 May 2007)

ABSTRACT

The oceanic response to overflows is explored using a two-layer isopycnal model. Overflows enter the open ocean as dense gravity currents that flow along and down the continental slope. While descending the slope, overflows typically double their volume transport by entraining upper oceanic water. The upper oceanic layer must balance this loss of mass, and the resulting convergent flow produces significant vortex stretching. Overflows thus represent an intense and localized mass and vorticity forcing for the upper ocean. In this study, simulations show that the upper ocean responds to the overflow-induced forcing by establishing topographic β plumes that are aligned more or less along isobaths and that have a transport that is typically a few times larger than that of the overflows. For the topographic β plume driven by the Mediterranean overflow, the occurrence of eddies near Cape St. Vincent, Portugal, allows the topographic β plume to flow across isobaths. The modeled topographic β-plume circulation forms two transatlantic zonal jets that are analogous to the Azores Current and the Azores Countercurrent. In other cases (e.g., the Denmark Strait overflow), the same kind of circulation remains trapped along the western boundary and hence would not be readily detected.

1. The interaction between the upper ocean and overflows

Marginal seas that have a topographically restricted exchange with the open ocean are favored places to form dense water in response to air–sea cooling and evaporation (Bryden and Stommel 1984). This dense water spills through the connecting strait and over the sill from the marginal sea into the open ocean as bottom-trapped gravity currents called "overflows" (Fig. 1). The Denmark Strait, the Faroe Bank Channel, the Mediterranean Sea, the Red Sea, and the Filchner Bank overflows are known to be major sources of deep water for the global ocean (Warren 1981).

a. How does the upper ocean interact with an overflow?

The importance of overflows in determining deep-ocean properties has been acknowledged for some time and has motivated efforts to understand their mixing dynamics (e.g., Whitehead et al. 1974; Candela 2001). But overflows must also affect the overlying oceanic layer. The Mediterranean overflow, for example, entrains about 2 Sv (1 Sv $\equiv 10^6$ m^3 s^{-1}) of overlying Atlantic Ocean water while descending the continental slope (Price et al. 1993). The presence of an overflow implies a localized mass loss for the upper ocean, so the upper oceanic layer must balance this mass loss and respond to the vortex stretching associated with entrainment. This aspect of overflow–upper ocean interaction has not been investigated much in the past, and indeed process models have often assumed the ambient ocean to be an inactive background field (Smith 1975; Baringer and Price 1997). This assumption leads to a greatly simplified model of the overflow (essentially, one active layer), but it certainly cannot be valid for the upper ocean.

* Current affiliation: International Pacific Research Center, University of Hawaii at Manoa, Honolulu, Hawaii.

Corresponding author address: Shinichiro Kida, IPRC, SOEST, 2525 Correa Rd., POST 401, University of Hawaii at Manoa, Honolulu, HI 96822.
E-mail: skida@hawaii.edu

DOI: 10.1175/2007JPO3750.1

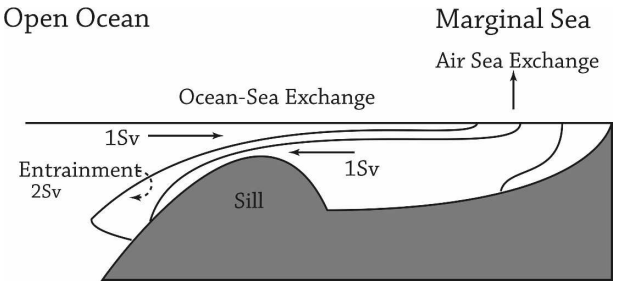

FIG. 1. A schematic of an overflow and its mass balance. The transport values are based on the Mediterranean overflow. Dense water that forms in the marginal sea spills over the sill as an overflow. This overflow (1 Sv) descends the continental slope, entrains overlying upper oceanic water (2 Sv), and reaches its neutral buoyancy level or the bottom. For the Mediterranean overflow, there is a flow of about 1 Sv from the Atlantic Ocean to the Mediterranean Sea in the upper layer. [Figure adapted from Price and Baringer (1994).]

Laboratory experiments have shown that overflows are capable of inducing a strong upper-layer motion (e.g., Whitehead et al. 1990; Etling et al. 2000), and three-dimensional primitive equation models also show overflows inducing an upper-layer motion through baroclinic instability (Jiang and Garwood 1996) and the formation of barotropic cyclones (Spall and Price 1998). Of most relevance here, Jia (2000) suggested that the formation of the Azores Current within an ocean general circulation model (GCM) depended on the presence or absence of a representation of the Mediterranean overflow–induced density field in the Gulf of Cadiz. The Azores Current is a zonal flow of 7–13 Sv in the upper ocean between 32° and 35°N (Stramma 1984; Klein and Siedler 1989; Alves and De Verdière 1999). It branches from the Gulf Stream and flows across the Atlantic Ocean as far eastward as the Gulf of Cadiz (Fig. 2). The GCM of Jia (2000) parameterized the Mediterranean overflow by imposing a sponge layer that restored the ocean-density profiles near the Strait of Gibraltar toward climatology (Levitus 1982). Thus the potential impact of an overflow on the large-scale upper-ocean circulation was established, though the dynamics of the upper ocean–Mediterranean overflow interaction were not revealed.

b. *Modeling the Mediterranean overflow and the overlying ocean*

The overflow and overlying ocean that are modeled in this paper are set in a parameter space close to that of the Mediterranean overflow in the Gulf of Cadiz. We use a two-layer isopycnal model, and the important bottom bathymetry used in the basic case experiment, hereafter case 1, is from Smith and Sandwell (1997). The boundaries are closed (Fig. 3), except where the Mediterranean overflow enters the open ocean with a transport of 1 Sv; the overflow then entrains 2 Sv of upper-ocean water near the Strait of Gibraltar. A reservoir created on the western end of the ocean basin balances mass in the model so that the total mass in each layer is conserved (see more details in the next section). The principal result (Fig. 3) is that this model of the Mediterranean overflow is found to establish a cyclonic circulation in the upper layer having a transport that is similar to the Azores Current and the Azores Countercurrent. This experiment thus indicates that an idealized Mediterranean overflow is indeed capable of inducing a significant upper-layer circulation that extends well into the open ocean.

c. *Observations of the Azores Current and the Azores Countercurrent*

The title Azores Current is usually applied to a zonal current that crosses (at least) the eastern half of the North Atlantic between 32° and 35°N (Fig. 2). The associated density field is known as the Azores Front and plays an important role in the subduction process in the eastern North Atlantic and its subtropical gyre (Rudnick and Luyten 1996; New et al. 2001). The position of the current is known to be a region of high eddy kinetic energy (Le Traon and De Mey 1994), which is thought to be a result of baroclinic instability (Kielmann and Käse 1987). The current is strongest near the surface and meanders with a wavelength of about 100 km and a phase speed of about 5 cm s^{-1}, close to that of a planetary Rossby wave. As the Azores Current approaches the eastern boundary, it bifurcates into a southward branch that joins the southward-flowing Canary Current and an eastward branch that flows into the Gulf of Cadiz. Paillet and Mercier (1997) estimated from an inverse model that the southward branch has a transport of about 6 Sv and the eastward branch about 4 Sv; our model results are consistent with this latter eastward branch.

The Azores Countercurrent is a westward current that is found to the north of the Azores Current at about 38°N (Onken 1993). The origin and the transport of this current are unclear, but Alves and De Verdière (1999) estimated its annual mean transport to be 2 ± 1 Sv using National Oceanographic Data Center hydrographic data. This is somewhat less than the transport associated with the Azores Current and not large compared with the mesoscale variability of transport (or dynamic height) observed in this region.

In the northern half of the Gulf of Cadiz, quasi-synoptic measurements appear to show a cyclonic up-

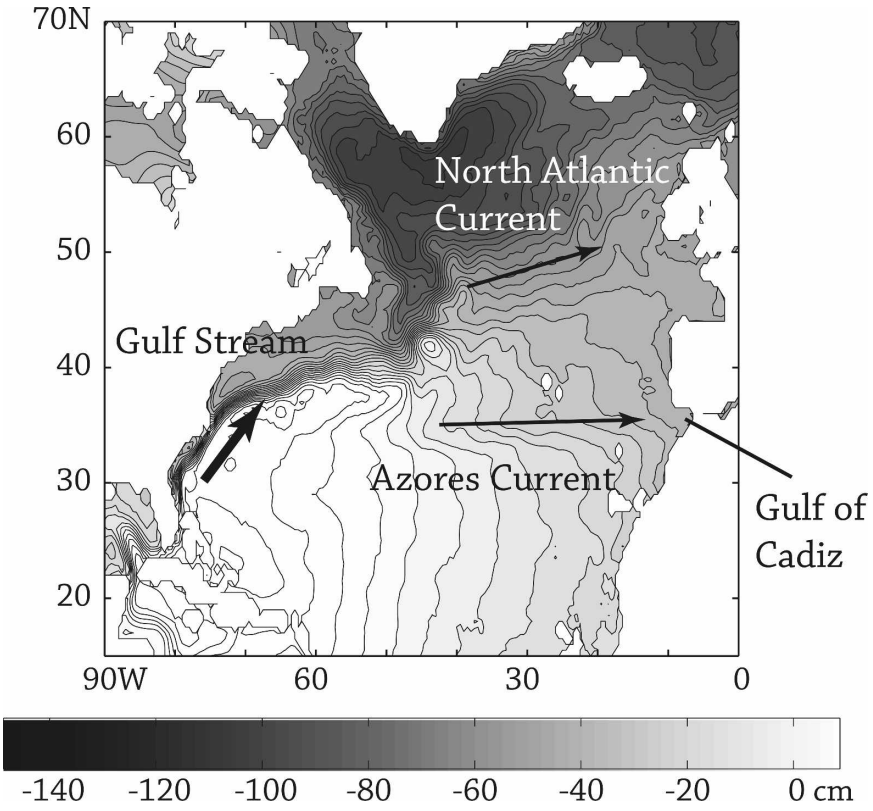

FIG. 2. The 1992–2002 mean ocean-dynamic topography calculated using joint data of satellite altimetry, near-surface drifters, National Centers for Environmental Prediction wind analysis, and Gravity Recovery and Climate Experiment (GRACE) satellite data (Maximenko and Niiler 2005). It shows the subtropical and subpolar gyres and the Azores Current. The data have been obtained from N. Maximenko (International Pacific Research Center) and P. Niiler (Scripps Institution of Oceanogrpahy). The Gulf Stream bifurcates at the tail of the Grand Banks into the North Atlantic Current (NAC) and the Azores Current. The NAC flows into the Nordic Sea and becomes part of the subpolar gyre. The Azores Current flows zonally across the Atlantic as a jet.

per-ocean circulation that may be connected to the Azores Current and the Azores Countercurrent. The absolute velocity measurements made during the Sortie des Eaux Mediterranean en Atlantique Nord–East (SEMANE) experiment show a westward flow at depths between 100 and 180 m above the Mediterranean overflow (Mauritzen et al. 2001). The geostrophic velocity field obtained in GOLFO 2001 also shows a similar westward flow above the Mediterranean overflow (Criado-Aldeanueva et al. 2006). Mauritzen et al. (2001) further estimated using hydrography data that this westward flow has a transport of about 4.6 Sv, while an eastward flow of about 7.7 Sv enters the Gulf of Cadiz in the interior. The eastward flow in the interior of the Gulf of Cadiz, with a transport larger than what is required to balance the mass lost to the Mediterranean overflow below, has also been observed by Ochoa and Bray (1991). In the southern half of the Gulf of Cadiz, a weaker anticyclonic circulation exists with a transport of about 1–2 Sv (Machín et al. 2006).

d. Hypotheses about the driving mechanism of the Azores Current

The following are two hypotheses about the driving mechanism of the Azores Current: The first is that the Azores Current is driven by wind stress. Käse and Krauss (1996) suggested that the Azores Current may be an extension of the Gulf Stream that flows along the weak wind-forced region of the subtropical gyre south to the line of zero wind stress curl. However, this transition region from subtropical to subpolar gyre appears too broad (±20°) to create and support a narrow jet like the Azores Current (±2°). GCMs also appear incapable of simulating the Azores Current from wind stress (Paiva et al. 2000; Jia 2000). The second hypoth-

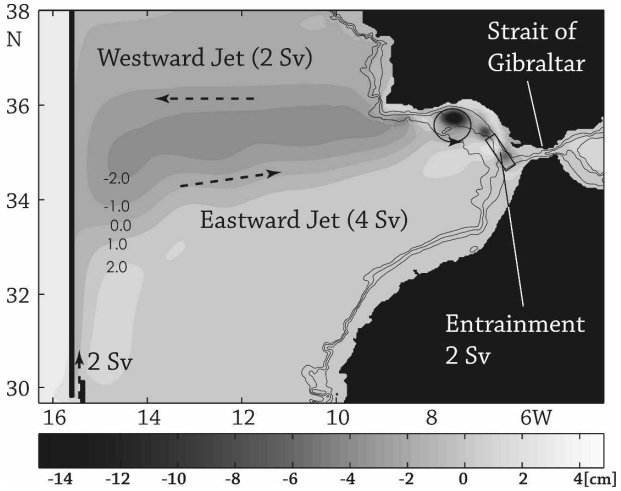

FIG. 3. A snapshot of the sea surface height for case 1 (shaded gray every 1 cm). The isobaths are contoured in black solid lines from 0- to 900-m depths every 300 m. Entrainment of 2.0 Sv is specified to occur within the rectangular boxed region near the Strait of Gibraltar between 300 and 600 m deep. The maximum depth in the Atlantic is 2000 m and is basically flat since seamounts are excluded for simplicity. Cyclonic eddies form along the northern part of the Gulf of Cadiz. An eastward zonal jet that forms between 34° and 36°N has a transport of 4.0 Sv and is analogous to the Azores Current; the westward zonal jet that forms between 37° and 38°N with a transport of 2.0 Sv is analogous to the Azores Countercurrent.

esis, first posed by Jia (2000), is that the Azores Current is driven by the Mediterranean overflow. Özgökmen et al. (2001) further suggested that the Azores Current is a branch of the planetary β plume driven by entrainment to the Mediterranean overflow. Their 1.5-layer reduced gravity model of the upper ocean showed an eastward jet of 10 Sv and a westward jet of 8 Sv, analogous to those observed for the Azores Current and the Azores Countercurrent. However, the match of the transport estimates in the model to observations is likely to have been a consequence of prescribing an entrainment region adjacent to the eastern boundary wall such that dissipative effects are of first-order importance. Absent this dissipation, the transport of a planetary β plume is estimated from the linear vorticity balance (Spall 2000) to be about 200 Sv, or more than an order of magnitude larger than the observations.

The hypothesis we pursue here amounts to a refinement of the second hypothesis noted above; namely, we know from observations (Price et al. 1993) that entrainment by the Mediterranean overflow occurs on a continental slope and not over the open ocean or adjacent to a vertical wall. Hence we test whether the Azores Current may be a branch of a *topographic* β plume rather than a *planetary* β plume. When the background potential vorticity (PV) gradient is dominantly controlled by the bathymetric slope, the transport of a linear topographic β plume (V) can be estimated as

$$V = \frac{f_o W}{\beta^* L_y}, \tag{1}$$

where W is the diapycnal transport, L_y is the length of the entrainment region across the slope, and β^* is the topographic β, which is $f_o\alpha/H$ with f_o, α, and H as the Coriolis parameter, slope, and mean upper-layer thickness, respectively. Reasonable parameter values are $f_o = 1 \times 10^{-4}\ \mathrm{s}^{-1}$, $L_y = 30$ km, $\alpha = 0.01$, and $H = 600$ m, so Eq. (1) estimates the transport of the topographic β plume driven by the Mediterranean overflow as 4 Sv (including the mass entrained to the overflow layer). Thus, the hypothesis that the Azores Current is a branch of the topographic β plume seems plausible, insofar as it gives a reasonable estimate of the transport. This, however, leaves open the question of how a topographic β plume could be connected to the open ocean and establish a zonal current such as the Azores Current.

e. *The goal and the outline*

The goal of this paper is to understand the basic dynamics of interaction between the upper ocean and an overflow, and specifically to explain the flow field of case 1, which we believe has an analog of the Azores Current. Outstanding questions include the following:

1) How does the upper ocean balance the mass loss caused by entrainment?
2) Can an overflow affect the upper ocean on a basin scale?

The first question is examined in section 2 using a comparatively simple and idealized ocean model (simple compared with a full GCM). The method for examining the overflow–upper-ocean interaction is the PV balance based on the concept of a β plume. The second question is examined in section 3, where we test the basin-scale impact of overflow–upper-ocean interaction and the hypothesis that the Azores Current is a branch of a topographic β plume. Summary and remarks will be presented in section 4.

2. The numerical model and idealizations of the bottom topography

The flow field of case 1 is complex in part because that experiment employs realistic bottom topography. To understand which aspects of the topography are

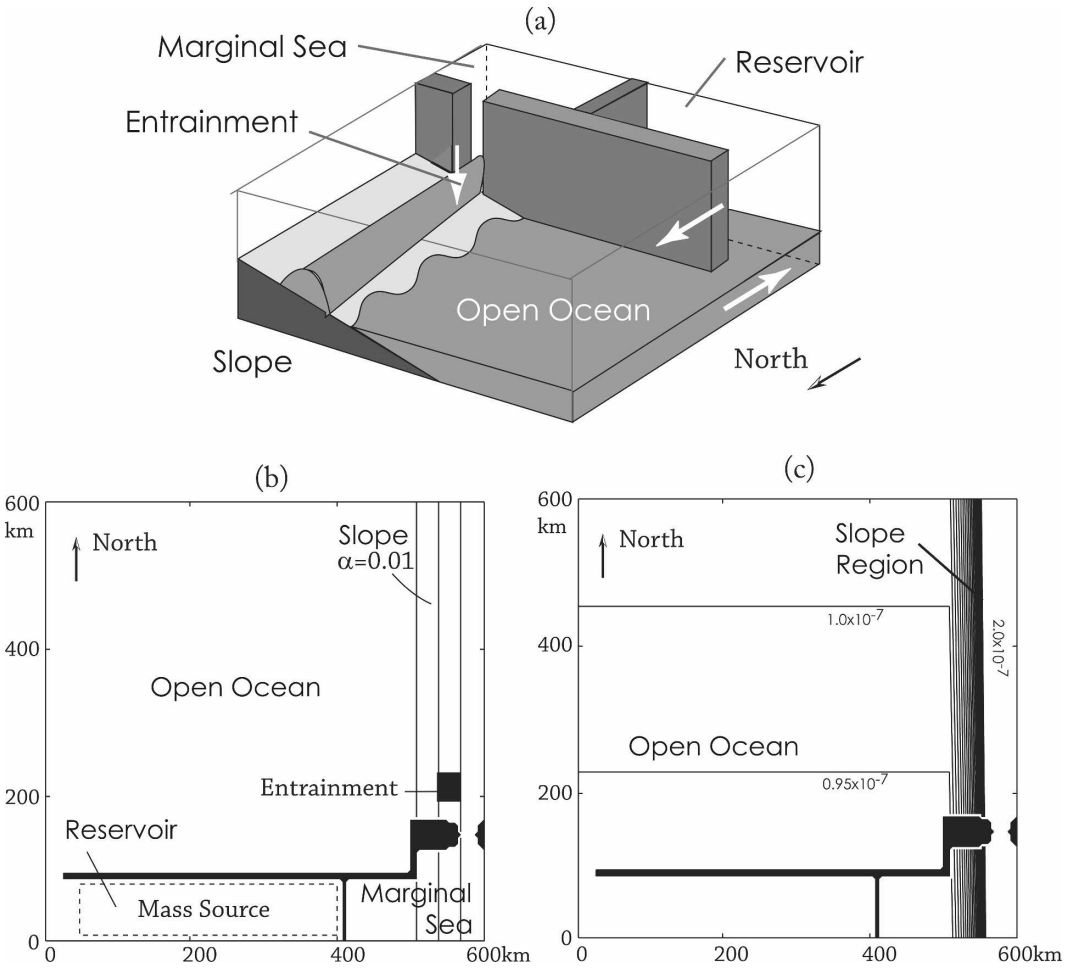

FIG. 4. (a) A schematic and (b) bird's-eye view of the model for case 2. There are three basins within the domain of 600 km × 600 km: the marginal sea, the open ocean, and a reservoir. The overflow enters the open ocean from the marginal sea through a narrow strait. The reservoir balances mass in each layer. The maximum depth in the open ocean is 2000 m and is flat. A continental slope of 0.01 is located along the eastern boundary of the open ocean, and its isobaths are drawn between 0- and 900-m depths every 300 m. Entrainment occurs within the black boxed region located near the strait. The interface in the open ocean is about 900 m. Note the change of the model orientation between the two figures. (c) The background PV contours for the upper layer contoured from 0.95 to 2.0×10^{-7} m^{-1} s^{-1} every 5×10^{-7} m^{-1} s^{-1}. PV contours are zonal in the open ocean (planetary β), but in the slope region they are basically along isobaths (topographic β). Note that the PV contours in the shallow part of the slope are not drawn since the PV values are significantly larger than those of the open ocean. The significant increase in the background PV gradient from the open ocean to the slope region can be noticed by the tightness of the contour lines.

most important, we have designed two idealizations of the continental slope topography. In case 2, described in this section, the continental slope is assigned a realistic value of 0.01, which is uniform along the entire eastern boundary of the ocean (Fig. 4). In case 3, described in section 3, the slope is increased downstream of the Strait of Gibraltar to represent the increase in bottom slope that occurs at about 8°W in the Gulf of Cadiz (Fig. 3). A basinwide upper-ocean circulation appears in this third case, and hence we conclude that bottom topography is of first importance for the overflow dynamics.

a. Details of the numerical ocean model

The numerical ocean model used in all three experiments is a two-layer isopycnal model built from the Hallberg isopycnal model (Hallberg 1997). The two layers represent the overflow and its overlying oceanic layers with a density difference of 0.5 kg m^{-3}, which represents that after entrainment (Price et al. 1993).

The interface between the overflow and upper oceanic layers is about 900 m in the open ocean, which is where the overflow is observed to stop its descent and become neutrally buoyant (Ambar and Howe 1979).

The domain is 600 km long meridionally and zonally with a resolution of 4 km. The earth's rotation is represented by a β plane that has f increasing to the north with $\beta = 2 \times 10^{-11}$ m^{-1} s^{-1}. The bottom topography for case 2 is flat and 2000 m deep over the open ocean, with a uniform slope of 0.01 along the eastern boundary (Figs. 4a,b), a representative value for the slope of the Gulf of Cadiz. For these parameters, the dominant background PV gradient is the planetary β in the open ocean region and topographic β in the continental slope region (Fig. 4c).

A marginal sea, located on the southeast corner of the open ocean, is connected to the continental slope region by a strait 16 km wide and 300 m deep. An overflow of 1.0 Sv exits the marginal sea into the open ocean. The isobaths are straight along the continental slope so that the overflow does not experience any curvature while flowing through the strait. This overflow is created by pumping 1.0 Sv of mass into the overflow layer within the marginal sea, while pumping an equivalent amount of mass out of the upper-ocean layer. To maintain constant volumes of both upper-ocean and deep- (overflow) ocean layers, a diapycnal mass flux of 2.0 Sv returns water from the deep layer to the upper oceanic layer within an oceanic reservoir situated on the southern edge of the open ocean (Fig. 4).

The overflow entrains 2.0 Sv of upper oceanic water in a specified region near the strait: 20–80 km downstream from the strait, between 300 and 620 m, and with a uniform diapycnal velocity ($w^* = 1.6 \times 10^{-3}$ m s^{-1}). In the real ocean, the location and the magnitude of entrainment depend on dynamics, but here we have prescribed the location and magnitude of entrainment based on the observations of Baringer and Price (1997).

Linear drag (bottom friction; $\upsilon = 7.5 \times 10^{-6}$ s^{-1}), Laplacian viscosity ($A_H = 10$ m^2 s^{-1}), and biharmonic viscosity ($A_{H4} = -8 \times 10^8$ m^4 s^{-1}) are used for friction, but the bottom friction will act only on the layer that directly contacts the bottom bathymetry. Biharmonic viscosity is used to dissipate the small-scale numerical noise of the overflow layer where its layer thickness is close to zero. Laplacian viscosity is used to effectively dampen the western boundary currents. Within 50 km from the western boundary, A_H increases exponentially from 10 to 1000 m^2 s^{-1} westward. Without this enhanced A_H near the western boundary, a strong inertial gyre develops and disrupts the interior flow field (Veronis 1966; alternatively, the inertial gyre could be avoided by greatly increasing the meridional domain size, which is computationally expensive). Note that friction is kept small outside the western boundary so that the dynamics in the ocean interior are not highly sensitive to the chosen frictional parameters.

b. *The formation of a trapped topographic β plume*

The instantaneous flow field of case 2 shows significant eddy variability. The upper layer responds to the overflow layer and entrainment by forming cyclonic and anticyclonic eddies (Fig. 5a). The cyclonic eddies have a sea surface height of -20 cm, a radius of 50 km, and a maximum azimuthal velocity of 10 cm s^{-1}. They are stronger and more numerous than the anticyclones that form on the inshore part of the continental slope because of the vortex stretching associated with entrainment. The overflow layer descends the slope roughly as expected from the frictional Ekman number while forming anticyclones (Fig. 5b).

The time-mean sea surface height shows the formation of a cyclonic topographic β plume along the continental slope with a transport of 3.3 Sv, roughly matching the estimate from Eq. (1) (Fig. 5c). The mean transport of this circulation appears to be largely controlled by the topographic β and is found to vary according to Eq. (1) as the magnitude of entrainment varies (Fig. 5d), although slightly less with the presence of the overflow layer below. The upper-ocean eddies are energetic, but nevertheless the mean transport of thickness $\overline{uh}$ is primarily carried by the mean flow $\overline{u}\,\overline{h}$ in this experiment. Thus, the response of the upper layer to an overflow in this case (and generally) is found to be the establishment of a topographic β plume.

Notice that this case 2 topographic β plume does not connect with the ocean interior and hence does not make an analog of the Azores Current. The large PV gradient set by the slope inhibits flow in the cross-slope direction and thus separates the slope region from the open ocean (Brink 1997). However, when an inertial overshoot occurs at the northern boundary, the topographic β plume does extend into the open ocean with an anticyclonic circulation to its south (Figs. 5a,c). Once the flow connects to the open ocean, the background PV gradient is mainly the planetary β, and so the flow becomes zonally oriented. These two gyres are established along the northern boundary of the model, unless the domain is made sufficiently large meridionally so that the background PV contours in the continental slope region are directly connected to the open ocean region (estimated to be about 1500 km).

This case 2 experiment shows that the basic upper oceanic response to overflows is to establish a topographic β plume with a transport that is a few times larger than that of the underlying overflow. The circu-

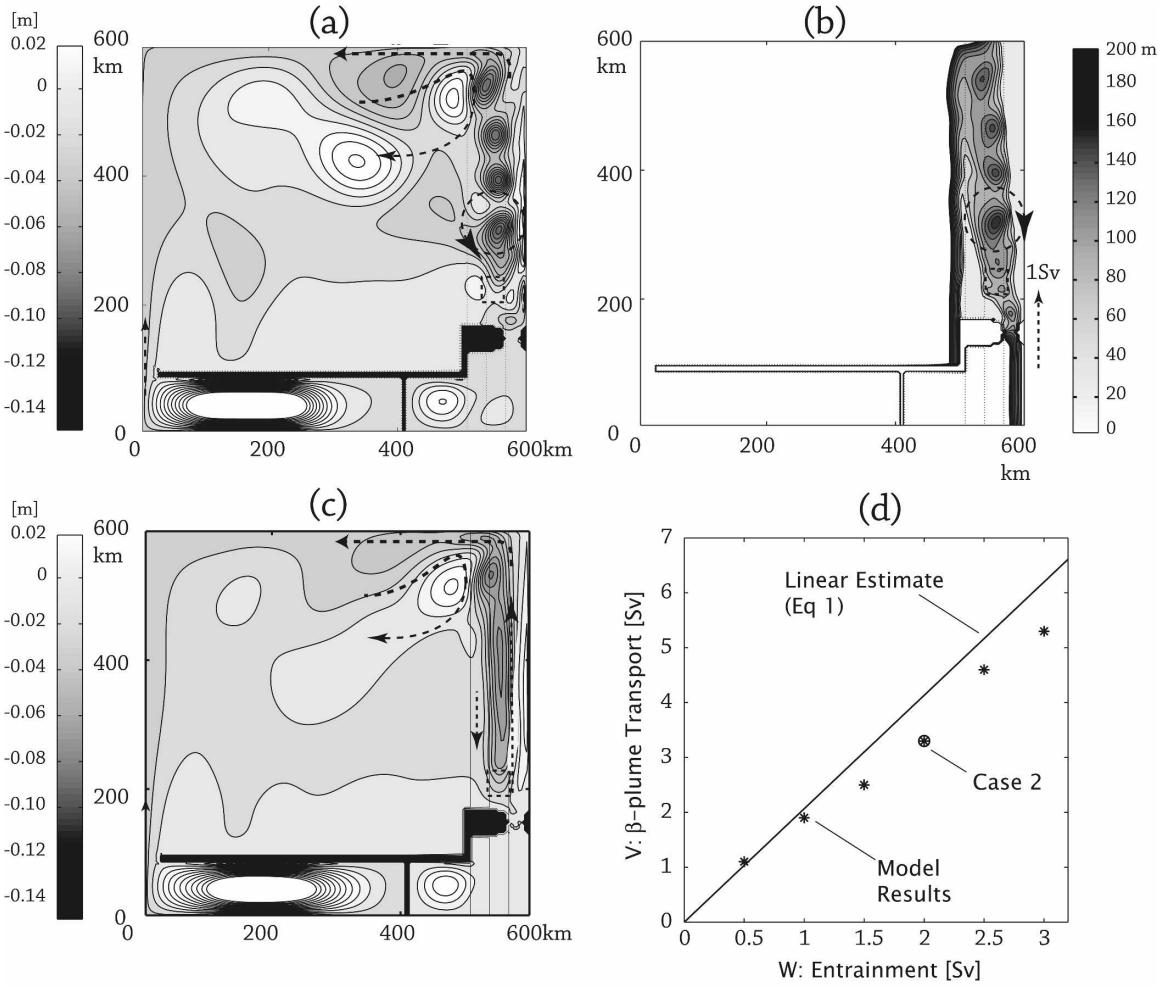

FIG. 5. (a)–(c) The flow fields of case 2. The isobaths are drawn from 0- to 900-m depths every 300 m. (a) A snapshot of the sea surface height contoured from −15 to 2 cm every 1 cm. Cyclonic eddies form along the continental slope. (b) A snapshot of the overflow-layer thickness contoured from 0 to 200 m every 10 m. The overflow descends the slope while forming anticyclonic eddies. (c) The time averaged sea surface height. A cyclonic topographic β plume forms along the continental slope (3.3 Sv) but extends into the open ocean at the northern boundary likely because of the inertial overshoot at the northern boundary. (d) The transport of the cyclonic topographic β plume, V, as a function of entrainment, W. As W increases, V increases approximately according to Eq. (1).

lation is aligned along the slope and remains trapped within the continental slope region for a meridional distance of O(1000 km). Evidently, something else is required for the topographic β plume to become a basin-scale flow, that is, to form an Azores Current.

3. The formation of a basin-scale topographic β plume

Next, the upper-ocean response to an overflow is examined in the presence of a slope change. This is the second feature recognizable in the continental slope of the Gulf of Cadiz (Fig. 3), and it will be shown here that this feature is essential for the topographic β plume to connect to the open ocean and to become a basin-scale flow.

a. The slope change and its effect

A region of steep slope is added to the model used in case 2 while keeping the coastline straight (Fig. 6):

$$h_b = 0.01(x - x_e)\left[2.5 - 1.5\tanh\left(\frac{y - y_c}{a}\right)\right], \quad (2)$$

where x_e is the location of the eastern boundary in x, a is the half-transitional scale of the slope change (20 km), and y_c is the location where the slope changes from 0.01 to 0.04 in y, which is about 150 km from the strait and is also the length scale from the Strait of

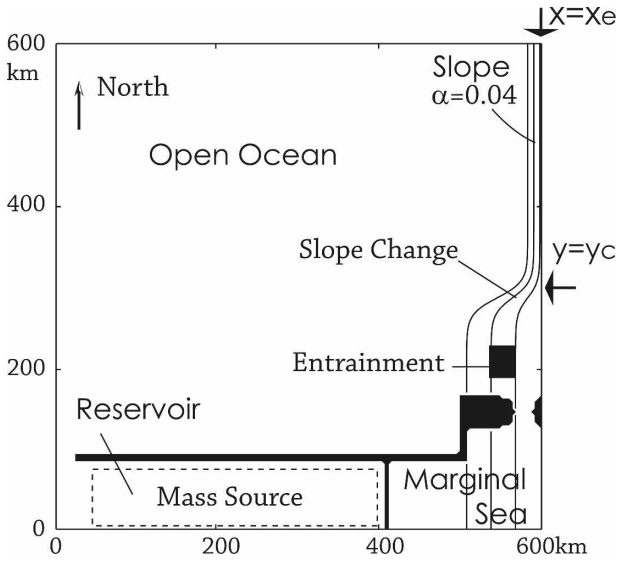

FIG. 6. A bird's-eye view of the model for case 3. The isobaths are drawn from 0- to 900-m depths every 300 m. The coastline of the continental slope along the eastern boundary is straight, but the slope changes from 0.01 to 0.04 at $y = y_c$, with a transitional scale of 40 km. All other setups are the same as in case 2 (Fig. 4).

Gibraltar to Cape St. Vincent. There is a curvature in the slope—an inevitable effect when the slope changes—but other experiments (Kida 2006) indicate that a flow with a small Rossby number is almost unaffected by this curvature. The open-ocean depth of 2000 m, the location of entrainment, and other parts of the model are exactly the same as in case 2.

The upper layer responds to entrainment by establishing a topographic β plume (Fig. 7a) similar to that observed in case 2 (Fig. 5) where the slope is gentle. A southward flow forms on the offshore side of the slope and a northward flow forms on the onshore side of the slope. However, the topographic β plume extends into the open ocean where the slope is steep. An eastward jet thus forms in the open ocean with a transport of 3.2 Sv and a width of 100 km, which is analogous to that formed in case 1 (Fig. 3). A westward flow also forms along the northern boundary with a transport of 1.2 Sv and a width of 200 km. Thus the slope change appears to be crucial for extending the topographic β plume into a basin-scale flow. Once the flow connects to the open ocean where planetary β is the dominant background PV gradient, the topographic β plume becomes zonally oriented and establishes the two zonal jets that look similar to the planetary β plume. While the flow in the upper layer becomes a basin-scale flow, the overflow remains trapped along the continental slope even after reaching a depth of 900 m (Fig. 7b). The overflow is still in direct contact with the continental slope and remains strongly controlled by the topographic β.

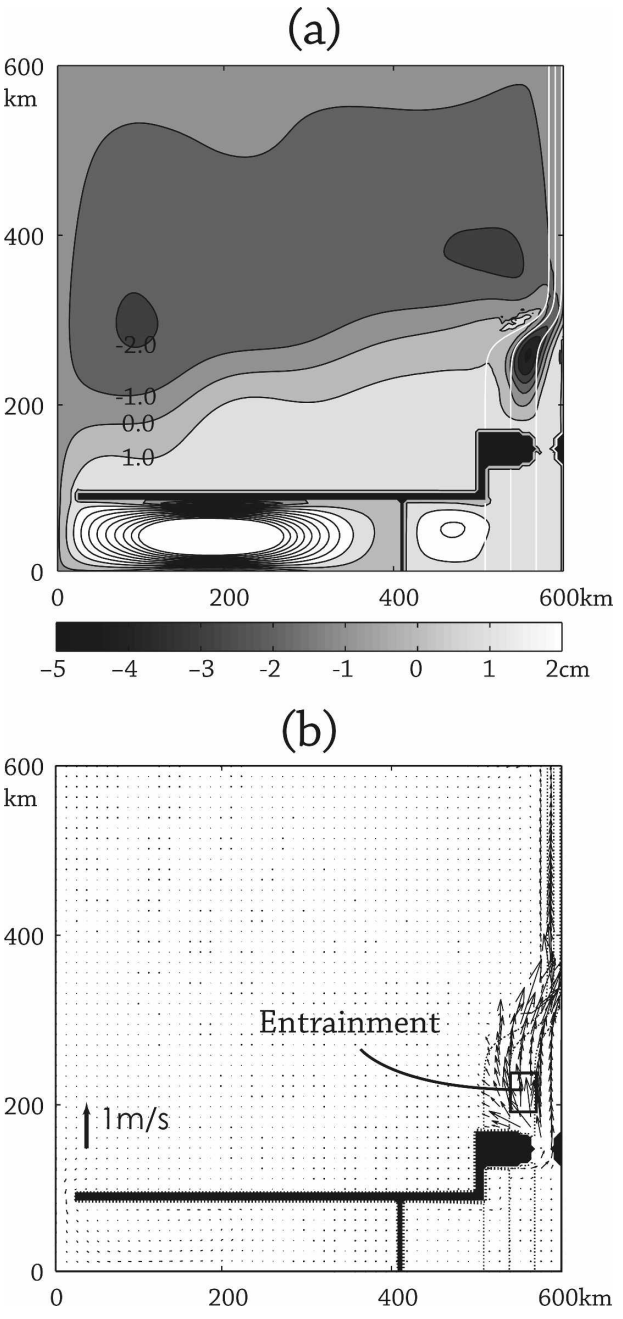

FIG. 7. The time-mean flow field for case 3. (a) The sea surface height is contoured from every 1 cm. Isobaths are drawn from 0- to 900-m depths every 300 m in white solid lines. A cyclonic topographic β plume forms along the continental slope where the slope is gentle, but the flow extends into the open-ocean interior where the slope is steep. As a result, an eastward jet of 3.2 Sv forms in the open ocean. (b) The time-mean velocity vectors of the overflow layer. Isobaths are drawn in black solid lines. The flow narrows where the slope is steep but still follows the isobaths in the steep-slope region.

b. The eddies and their role in the slope-transition region

What processes are responsible for connecting the topographic β plume to the open ocean? The processes can be revealed from the full PV equation of the upper oceanic layer:

$$\overline{\mathbf{U_1}} \cdot \nabla \overline{q_1} = \overline{q_1} w^* - \nabla \cdot \overline{\mathbf{U}_1' q_1'} + \hat{k} \cdot \nabla \times \overline{\mathcal{F}_1}, \qquad (3)$$

where $\boldsymbol{U}$ is the transport, q is the PV, $\mathcal{F}$ is the friction, an overbar represents the time mean, and the prime represents fluctuation, with subscript 1 used for the values for the upper layer. The mean background PV gradient $\nabla \overline{q}_1$ is largely controlled by the slope:

$$\nabla \overline{q}_1 \simeq \overline{\left(\frac{q_1 \nabla h_b}{h_1} \right)}. \qquad (4)$$

The term on the left-hand side of Eq. (3) represents PV advection due to a flow across isobaths. The three terms on the right-hand side of Eq. (3), PV forcing ($\overline{q_1} w^*$), eddy–PV flux divergence ($\nabla \cdot \overline{\mathbf{U}_1' q_1'}$), and friction ($\hat{k} \cdot \nabla \times \overline{\mathcal{F}_1}$), are the three processes in this model that can induce a flow across isobaths.

For case 3, the dominant PV balance in the entrainment region is between the PV forcing and the PV advection terms (Figs. 8a–d). But in the steep-slope region, the dominant balance is between the PV advection term and the eddy–PV flux divergence term. Friction is significant only adjacent to the eastern boundary. The PV balance shows that eddies allow the topographic β plume to flow across isobaths and become a basin-scale flow. Examining the eddy–PV flux using the quasigeostrophic (QG) approximation (which is valid here) reveals that the eddies in the slope-transition region are found to play a role that can be interpreted qualitatively as viscosity. Under the quasigeostrophic approximation, the eddy–PV flux divergence term can be divided into a Reynolds stress term (the eddy-momentum flux along isopycnals) and a form drag term (eddy-momentum flux across isopycnals; Rhines and Holland 1979; Plumb 1986). For case 3, the main component of the eddy–PV flux is the Reynolds stress:

$$\frac{\text{form drag}}{\text{Reynolds stress}} = \frac{f u' h'/H_1}{u' \zeta'} = \frac{fL}{u'} \frac{h'}{H_1}. \qquad (5)$$

Substituting $u' = 0.2$ m s^{-1}, $L = 20$ km, $h' = 10$ m, and $H_1 = 600$ m, which are the representative values for the eddies in the steep-slope region, Eq. (5) gives an estimate of 0.17. Furthermore, the Reynolds stress in the cross-slope direction, which is the main component for the eddy–PV flux divergence, shows that the eddies are moving momentum down the mean gradient of the flow (across slope). Thus, the eddy–PV flux divergence term can be represented approximately as momentum diffusion, that is, something like a viscosity times the mean gradient:

$$\overline{\mathbf{U}_1} \cdot \overline{\left(\frac{q_1 \alpha}{h_1} \right)} = -\nabla \overline{\mathbf{U}' q'} \simeq -\frac{\partial}{\partial x} \overline{u' \zeta'} \simeq \frac{\partial}{\partial x} \left(A_H^* \frac{\partial \overline{\zeta}}{\partial x} \right), \qquad (6)$$

where x is the direction perpendicular to isobaths and A_H^* is the "effective" viscosity due to eddies, often termed "eddy viscosity coefficient." Here, A_H^* is estimated to be about 460 m^2 s^{-1} where the slope changes from gentle to steep (Fig. 8e). The reason for such a strong down-gradient vorticity transfer in the slope-transition region may be due to geometric changes in the eddy size or additional instability where the slope changes abruptly (Bracco and Pedlosky 2003), but further investigation is required to understand this.

The experiment of case 3 shows that the topographic β plume will become a basin-scale flow in the presence of a steep slope. Enhanced dissipation by eddies enables the topographic β plume to flow across isobaths and connect to the open ocean.

c. The lateral Ekman number and the topographic β plume

The enhanced dissipation created by eddies in the slope-transition region appears to be the essential process that causes the topographic β plume to connect to the open ocean (Fig. 7b); without this enhanced dissipation, the topographic β plume likely remains on the slope, as observed in case 2 (Fig. 4c). The role of dissipation can be modeled as an eddy viscosity that diffuses the topographic β plume offshore. The magnitude can be diagnosed from the lateral Ekman number γ, the angle of the flow crossing the isobaths (Fig. 9a). A flow with a large γ will flow across isobaths with a steeper angle than a flow with a small γ. Thus γ represents the effect of the eddy viscosity on changing the PV of a water column, which is otherwise flowing in the along-slope direction.

The linear-vorticity balance of Eq. (6) (Pedlosky 1974) is used to estimate the lateral Ekman number:

$$\frac{f\alpha}{H_1} u = A_H^* \frac{\partial^3 v}{\partial x^3}, \qquad (7)$$

where H_1 is the mean upper oceanic layer thickness in the continental slope region and overbars are neglected from u and v (Fig. 9b). Here, A_H is assumed constant, and its variance will be discussed later. This linear-vorticity balance Eq. (7) is then seen to be a balance

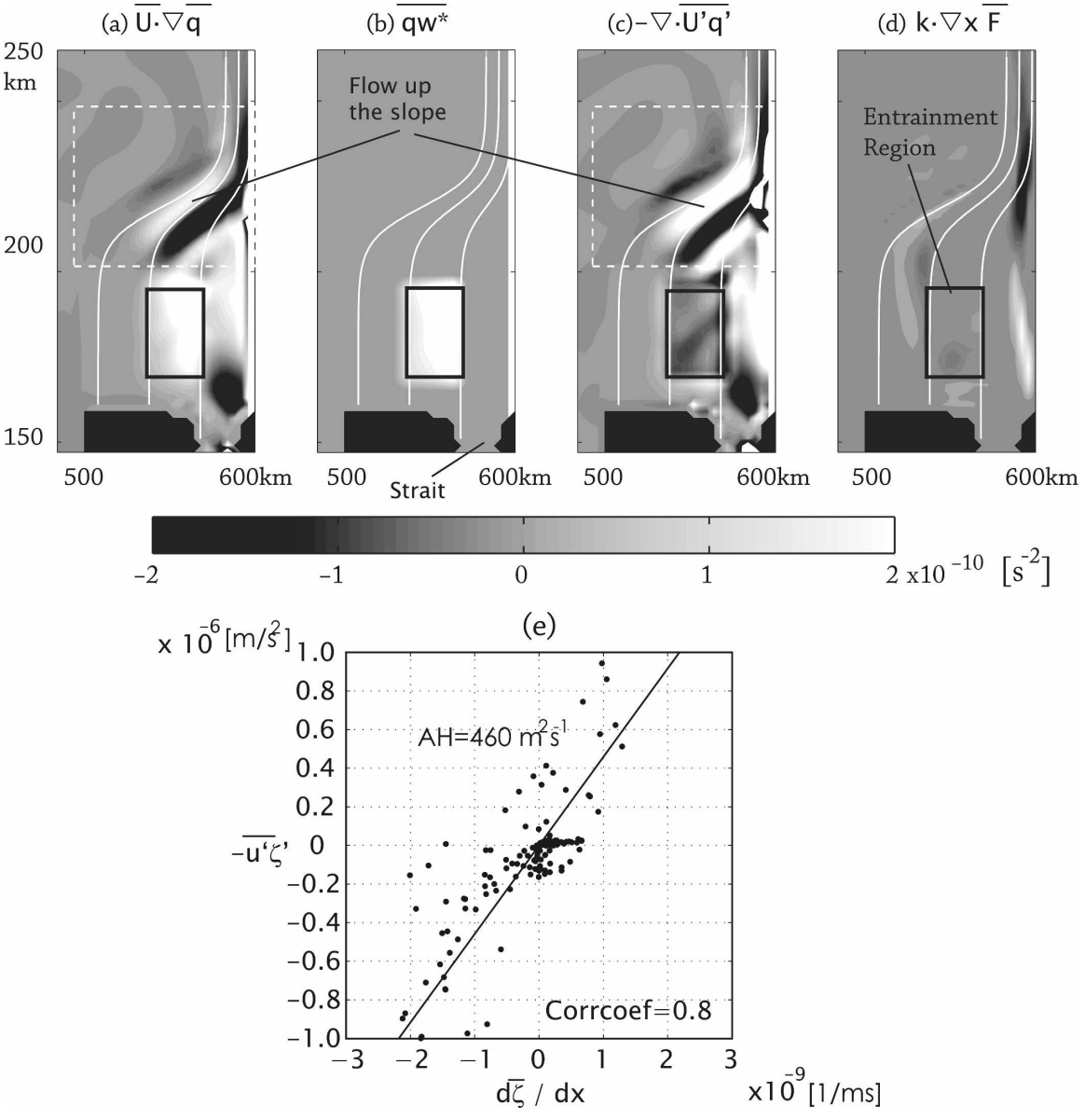

FIG. 8. The PV balance [Eq. (3)] near the slope-transition region: (a) PV advection, (b) PV forcing, (c) eddy–PV flux divergence, and (d) PV dissipation. The dominant balance in the slope transition region is between the PV advection and the eddy–PV flux divergence. (e) The Reynolds stress in the across-slope direction $-\overline{u'\zeta'}$ plotted against the mean vorticity gradient across slope $\overline{\zeta}_x$ where the slope varies from gentle to steep. The ratio of the two terms $-\overline{u'\zeta'}/\overline{\zeta}_x$ is the estimate of A_H^* for each point; thus the slope for the best line fit is the rough estimate for A_H^* in the region. There is reasonable correlation between the two terms (a correlation coefficient of 0.8), and A_H^* is estimated to be about 460 m^2 s^{-1}.

between the mean PV advection (the left-hand side) and the convergence of the viscous flux of the relative vorticity associated with the flow in the along-slope direction (the right-hand side). By taking the width scale of the flow ∂x to be half the mass sink (external forcing) size $X_o/2$, Eq. (7) can be scaled and then solved for u/v, which is the angle of flow across the slope and also the lateral Ekman number γ:

$$\gamma \equiv \frac{u}{v} = \frac{A_H^* H_1 \alpha^2}{f_o \delta h^3}. \tag{8}$$

Here, X_o is eliminated from this equation using $\delta h = \alpha(X_o/2)$, the topographic depth difference across the flow. Equation (8) shows that γ will increase quadratically as the slope increases, provided that A_H^* is a constant and not dependent on the slope. So even if A_H^* is

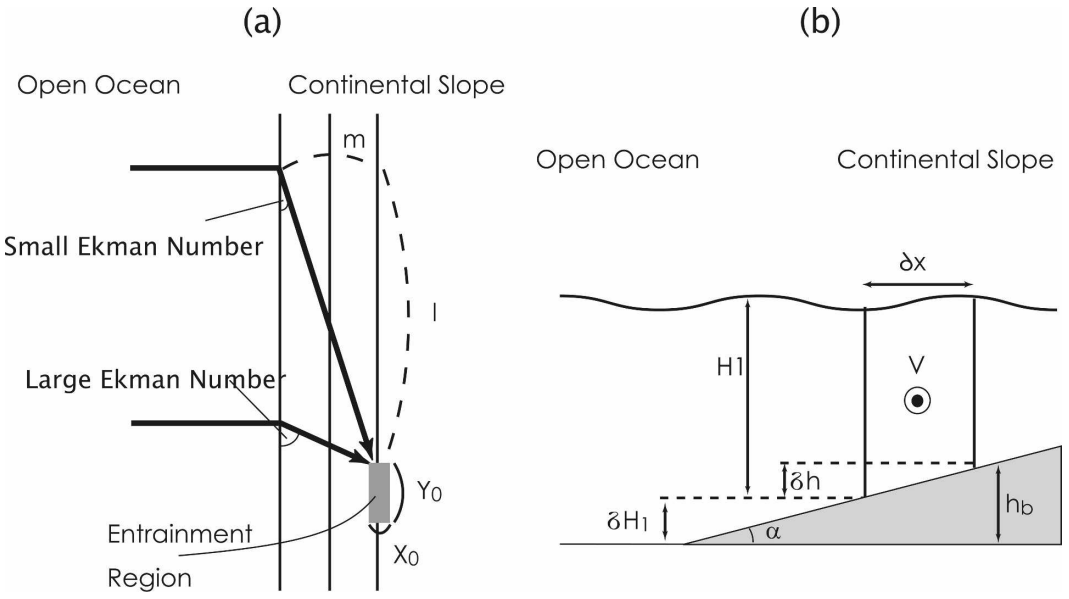

FIG. 9. (a) A schematic of the incoming (east–southward) branch of the topographic β plume between the entrainment region and the open ocean. The entrainment region has a size of X_o by Y_o. The zonal distance between the entrainment region and the open ocean is m, and the meridional distance between the entrainment region and the eastward jet in the open ocean is l, which decreases as the Ekman number γ increases. (b) A schematic of the incoming (east–southward) branch of the topographic β plume on a slope. Here, h_b is the bottom bathymetric height, H_1 is the basic upper-layer thickness of the flow in the continental slope region, and δH_1 is the thickness difference between the entrainment region and the open-ocean region. The cross-slope width of the flow is ∂x, and δh is the difference of the flow thickness within the flow.

the same, a flow will cross the slope at a steeper angle if the slope is itself steeper.

If γ is known, the location where the topographic β plume will connect to the open ocean can be estimated (Fig. 9a). We will focus on the incoming (east–southward) branch of the topographic β plume because this branch becomes the flow that is analogous to the Azores Current. Although the flow is eastward, the planetary Rossby waves that establish the open-ocean flow travel westward from the slope region to the open ocean. Taking the distance between the entrainment region and the open ocean to be m, the distance l required for the flow to connect to the open ocean is

$$l = \frac{m}{\gamma} = \frac{f\delta h^3 \delta H_1}{A_H^* H_1 \alpha^3}, \tag{9}$$

where δH_1 is the upper-layer thickness difference from the entrainment region to the open ocean and Eq. (8) is substituted for γ. This scale estimate in Eq. (9) shows that l decreases proportionally as the inverse cube of α, a similar behavior as the arrested topographic wave on an f plane (Csanady 1978). Although the background PV gradient will increase with α, the length scale in the cross-slope direction will also increase with α. It is this latter effect that dominates and thus leads to a decrease in l as α increases.

A linear, barotropic single-layer model is used to test whether Eq. (9) gives a fair scale estimate of l. This model represents only the upper oceanic layer and neglects the overflow layer, so that the maximum depth in the open ocean is 900 m and the single moving layer is in direct contact with the slope in the continental slope region. Eddies are parameterized as a viscosity-like term, and A_H^* is temporarily set to 10 $m^2\ s^{-1}$, the background viscosity coefficient used in cases 1–3. The strength and the location of the mass sink in this model are exactly the same as in case 2. As expected, the topographic β plume will not connect to the open ocean when the slope is gentle (0.01) and constant and when the meridional extent of the model is small (Fig. 10a). When the meridional size of the model is increased to 2000 km, a broad eastward flow forms, centered at about 800 km from the entrainment region; as the slope is increased, l is found to decrease roughly according to Eq. (9) (Fig. 11). Note that the depth range of the entrainment region (between 300 and 600 m deep) and the maximum open-ocean depth (900 m) are kept fixed, but the slope varies so that the PV difference between the entrainment region and the open ocean remains the

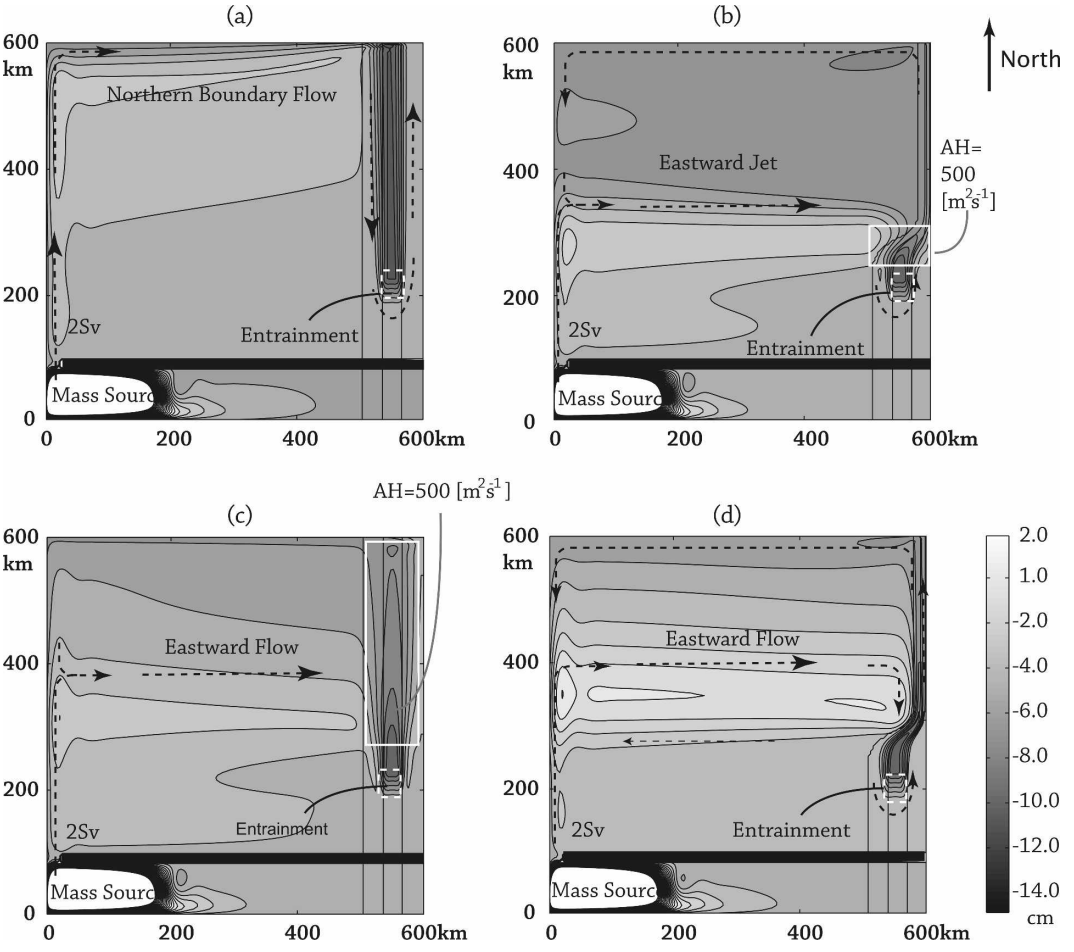

FIG. 10. Sea surface height contoured from −15 to 15 cm every 1 cm from four idealized experiments using the linear barotropic model. The isobaths are drawn from 0- to 900-m depth every 300 m. (a) Constant gentle slope of 0.01 similar to case 2. The topographic β plume forms along the continental slope and is not connected to the open ocean. (b) Continental slope similar to case 3 with a uniform $A_H^* = 10\ \mathrm{m^2\ s^{-1}}$ across the basin, except where the slope changes from gentle to steep (white-square boxed region). There, $A_H^* = 500\ \mathrm{m^2\ s^{-1}}$ is used. The eastward zonal jet forms in the open-ocean region about 60 km from the entrainment region, similar to where it forms in case 3. (c) Constant gentle slope of 0.01 similar to case 2, but A_H^* changes from 10 to 500 $\mathrm{m^2\ s^{-1}}$ exponentially, about 60 km north of the entrainment region (white-square boxed region). An eastward flow forms that is centered about 200 km to the north of the entrainment region but is broader thanthat observed in (b). (d) Continental slope similar to case 3, but with a uniform A_H^* of 10 $\mathrm{m^2\ s^{-1}}$. A broad eastward flow forms in the open-ocean region that is centered about 120 km north of the entrainment region.

same in all experiments. When the slope is fixed to 0.01 and A_H^* is varied instead, l is found to decrease proportionally as the inverse of A_H^*, also according to Eq. (9) (Fig. 11). Thus the linear barotropic model shows that when the basic vorticity balance is the linear balance [Eq. (7)], Eq. (9) does give a fair estimate of l and the location where the zonal jet forms.

The topographic β plume in case 3 likely connects to the open ocean with a small l because of the significant increase of γ in the slope-transition region due to large α and A_H^*. Based on Eq. (9), l is estimated to be less than 10 km when the slope is 0.04. This small l matches the result in case 3, where the eastward zonal jet forms close to the slope-transition region (Fig. 7a). A narrow zonal jet is indeed observed to form at the latitude of the slope-transition region also in the linear barotropic model, which is similar to case 3 when A_H^* is locally increased to 500 $\mathrm{m^2\ s^{-1}}$ in the slope-transition region, so that A_H^* in the linear barotropic model will roughly mimic the role of eddies in case 3 (Fig. 10b). In the rest of the basin, A_H^* is 10 $\mathrm{m^2\ s^{-1}}$. It is worth stressing that the significant increase in γ is a result of an increase in both α and A_H^*. A large increase in A_H^* alone cannot create a narrow zonal jet in the open ocean. When A_H^*

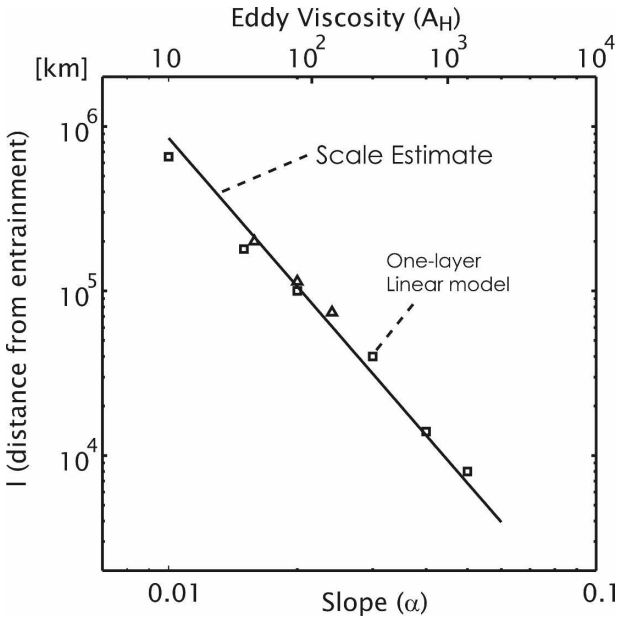

FIG. 11. The meridional distance l between the eastward jet and the entrainment region plotted against the slope α (bottom scale) and the eddy viscosity coefficient A_H^* (top scale). Here, l decreases when α increases (triangle) or when A_H^* increases (square). Both results show that distance decreases approximately according to the scale estimate of l obtained using Eq. (9) (solid line).

increases from 10 to 500 $m^2\ s^{-1}$ in about 40 km but with the slope kept constant (0.01), an eastward zonal flow forms in the open ocean interior that is farther north and broader than that found in case 3 [Fig. 10c; this increase in A_H^* occurs exactly on the same spatial scale as the slope change a in Eq. (2)]. Additionally, a steep slope alone cannot create a narrow zonal jet in the open ocean. When α increases from 0.01 to 0.04 exactly as Eq. (2) exhibits but with A_H^* kept constant (10 $m^2\ s^{-1}$), an eastward zonal flow forms in the open ocean interior that is farther north and broader than that found in case 3 (Fig. 10d).

An additional offshore diffusion of the topographic β plume may have occurred in case 3 also because of the spatial variation of A_H^*. When A_H^* varies spatially, the eddy-viscosity term is a sum of two terms:

$$\frac{\partial}{\partial x}\left(A_H^*\frac{\partial}{\partial x}\bar{\zeta}\right) = A_H^*\frac{\partial^2\bar{\zeta}}{\partial x^2} + \frac{\partial A_H^*}{\partial x}\frac{\partial\bar{\zeta}}{\partial x}. \qquad (10)$$

Note that the second term of Eq. (10) is zero if A_H^* is a constant. However, when A_H^* varies in the across-slope length scale similar to the length scale of the topographic β plume, the two terms on the right-hand side of Eq. (10) may be of similar magnitude. This spatial variability of A_H^* can thus change the effectiveness of eddies in diffusing the topographic β plume offshore.

4. Summary and remarks

The goal of this paper is to better understand the interaction between an overflow and the upper ocean, with some emphases on the latter. At the outset we identified two outstanding questions and here we review our responses:

1) *How does the upper oceanic layer balance the mass loss caused by entrainment into the overflow?* In highly resolved model solutions, the upper ocean responds to entrainment by establishing a cyclonic circulation over the continental slope region. For typical values of bottom slope, this β plume is aligned along isobaths because the background PV gradient is largely caused by the topographic β rather than by the planetary β. The large difference of PV between the continental slope and the open-ocean regions tends to inhibit flow in the across-slope direction.
2) *Can overflows affect the upper ocean over a basin scale, as opposed to the comparatively small continental slope scale of the overflow?* Dissipation (friction) can allow the topographic β plume to cross isobaths (PV lines). Dissipation is enhanced considerably by the presence of mesoscale eddies and by a steep continental slope. When these are present in a model solution, which requires a very high horizontal resolution compared with that possible in most ocean GCMs, the topographic β plume driven by the Mediterranean overflow is found to connect to the open Atlantic by establishing two zonal jets, essentially a planetary β plume, though with transport that is characteristic of the topographic β plume. On this basis, the hypothesis that entrainment by the Mediterranean overflow is the principal driving agent for the Azores Current seems highly plausible.

a. *Comparing other features of the case 1 solution with observations*

The size and magnitude of the cyclonic eddies forming in the upper layer of the northern half of the Gulf of Cadiz in case 1 (Fig. 3) are analogous to those observed near the surface adjacent to Meddies (Carton et al. 2002). Whether the cyclonic eddies outnumber the anticyclonic eddies in the real ocean remains unclear, but the high time variability observed in the northern side of the Gulf of Cadiz from satellite altimetry (Høyer et al. 2002) may be another indication of the high eddy activity in the overflow region. The time variability of 7–8 days observed in the overflow layer of the model is also similar to the 7–9-day period time variability observed at Portimão Canyon, Portugal (Chérubin et al. 2003).

The westward zonal jet, having a width of about 100 km and a transport of about 2 Sv that forms in case 1 near 38°N (Fig. 3), is perhaps analogous to the Azores Countercurrent. Although observations of this current are unclear, these results suggest that the formation of such a current is a direct result of the topographic β plume driven by the Mediterranean overflow. To observe the westward flow within the Gulf of Cadiz, a monitoring of the velocity field for more than a few days is necessary since the transient eddy flow field is likely overwhelming. Some investigators have proposed that the Azores Countercurrent may be driven by the eddies created by the Azores Current that are caused by baroclinic instability (Alves et al. 2002). This eddy-driven mechanism will establish two westward countercurrents, north and south of the Azores Current, wherever the Azores Current is unstable. In contrast, the formation of a westward countercurrent by the topographic β plume will only create one countercurrent, to the north of the Azores Current, which originates from the eastern boundary. The two mechanisms (topographic β plume and baroclinic instability) may very well coexist, but further observations are required to know if either prevails.

b. *Future directions*

The model used in this paper simplifies several features of the real ocean, including entrainment dynamics, which were here specified. Since this process is an area of intensive ongoing research, we will emphasize three other possible areas for extension of this study: the effects of stratification, the exchange flow at the Strait of Gibraltar, and wind stress over the open ocean.

1) STRATIFICATION

The zonal jets in cases 1 and 3 are fairly steady, but additional calculations with more layers and thus more realistic stratification have shown greater time variability due to baroclinic instability as more layers are added (more realistic stratification). The present two-layer solutions satisfy the necessary condition for baroclinic instability but with a slow growth rate, about 100 days based on Phillips's model (Pedlosky 1987); strong time variability was not observed in cases 1 and 3. By comparison, the actual Azores Current has an estimated growth rate for baroclinic instability of about 8 days (Kielmann and Käse 1987). This great difference in growth rate arises because the speed of the zonal currents is underestimated in our two-layer solutions even if the transport is realistic. More time variability is expected as more realistic stratification is included and the zonal jets become more strongly surface intensified.

2) EXCHANGE FLOW

An upper-ocean transport of a little less than 1.0 Sv enters the Mediterranean Sea from the Atlantic (Bryden and Stommel 1984). This upper-layer inflow to the Mediterranean Sea was not included in the present model experiments so as to isolate the effect of overflows on the upper ocean. Additional calculations that include this inflow show that the transport of the westward branch of the topographic β plume weakens by a little less than 1.0 Sv, while the eastward branch is largely unaffected. The interaction between the two flows is likely inhibited because of the significant PV difference between them. Compared to the water mass that is entrained into the Mediterranean overflow, the water mass that flows into the Mediterranean Sea is considerably shallower and less dense.

3) THE WIND-DRIVEN GYRE

Perhaps the biggest feature that is missing from our model is the wind-driven gyre, which may interact with the topographic β plume on a very large scale in the open ocean. The transport of the Azores Current that enters the Gulf of Cadiz is estimated to be about 4.0 Sv (Paillet and Mercier 1997), which is what we find here, but this is about half of the Azores Current transport observed in the open ocean, 7.0–13.0 Sv (Gould 1985; Klein and Siedler 1989). Could this difference of 3.0–8.0 Sv be a result of the interaction between the topographic β plume and the wind-driven gyre? Observations (Fig. 2) and data-assimilation experiments (Gebbie 2004) indicate that the Sverdrup interior is mostly meridional at these latitudes, so that a simple superposition of the topographic β plume onto the wind-driven gyre would create a zonal kink to the sea surface height contours but would not be expected to enhance the zonal transport. The transport enhancement could perhaps be a result of eddy-driven mean flow associated with baroclinic instability of the Azores Current. For now, though, the question of why the Azores Current has a transport of about 8.0–13.0 Sv in the open ocean is not answered in this study.

c. *Closing remarks*

Among the five major overflows noted in the opening section, the Mediterranean overflow appears to be the only one that is likely to exert this more or less direct β-plume effect on the upper ocean on a basin scale. The Faroe Bank Channel overflow is on a northern boundary, so the PV contours created by the continental slope roughly coincide with those of the planetary PV contours. The topographic β plume is thus likely to be trapped within the continental slope. The Denmark Strait and Filchner Bank overflows exist on the western boundary, so there is no open ocean to the

west into which the topographic β plumes can expand. Moreover, the energetic western boundary currents around these overflows are likely to be overwhelming. The strong cyclonic eddies in the upper oceanic layer that form in our experiments are somewhat analogous to the ones observed downstream of the Denmark Strait (Bruce 1995), though there are other hypotheses for the formation of such cyclones (e.g., Lane-Serff and Baines 1998; Spall and Price 1998). The topographic β plume associated with the Denmark Strait overflow may also continue along the continental slope of Greenland and extend into the Labrador Sea. This scenario qualitatively matches with the numerical model result by Käse et al. (2001), which showed that the Denmark Strait overflow plays an important role in the formation of the narrow cyclonic circulation along the western boundary of Greenland and the Labrador Sea (Lavender et al. 2005). However, further experiments are required for a more detailed comparison. The Red Sea overflow is unlikely to establish a topographic β plume because entrainment occurs over a length scale of about 5 km, which is much smaller than the deformation radius (about 50 km; Özgökmen et al. 2003), and thus the dynamics are unlikely to be governed by the rotation of the earth.

The current state-of-the-art climate models and OGCMs have well-known difficulties reproducing the observed temperature and salinity structures in the regions where overflow waters are dominant (Gnanadesikan et al. 2006). Part of the difficulty is in the parameterization of entrainment by overflows, which has been a topic of intensive research (Price and Yang 1998; Legg et al. 2006). This study suggests that parameterization of overflows should include not just entrainment but also the effect of the vortex stretching on the upper layer for at least some overflows, almost certainly the Mediterranean overflow for the reasons noted above. An entrainment parameterization that places entrainment over the open ocean (not directly on a boundary) will result in vortex stretching, assuming only volume continuity. Indeed, a new, high-resolution regional simulation with such an entrainment parameterization has shown that the Mediterranean overflow is capable of forcing an Azores Current (Peliz et al. 2007). However, an entrainment parameterization placed on a side wall, for example, the marginal sea boundary condition of Price and Yang (1998), may need to be extended to account for vorticity consequences. Of course, even if a semiexplicit treatment of overflows is not possible in a given OGCM because of limited resolution, it may nevertheless be helpful to know that an Azores Current should not be expected if an entraining Mediterranean overflow is missing.

Acknowledgments. The authors thank Drs. Karl Helfrich, Sonya Legg, Amy Bower, and Raffael Ferrari as well as two anonymous reviewers for many useful comments. We are also grateful to Dr. Bob Hallberg of NOAA/GFDL for allowing us to use his isopycnal coordinate model, HIM. SK's support during the time of his Ph.D. research in the MIT/WHOI Joint Program was provided by the National Science Foundation through Grant OCE04-24741. JP and JY have also received support from the Climate Process Team on Gravity Current Entrainment, NSF Grant OCE-0611530.

REFERENCES

Alves, M. L. G. R., and A. C. De Verdière, 1999: Instability dynamics of a subtropical jet and applications to the Azores front current system: Eddy-driven mean flow. *J. Phys. Oceanogr.,* **29,** 837–864.

——, F. Gaillard, M. Sparrow, M. Knoll, and S. Giraud, 2002: Circulation patterns and transport of the Azores Front-Current system. *Deep-Sea Res. II,* **49,** 3983–4002.

Ambar, I., and M. R. Howe, 1979: Observations of the Mediterranean outflow. I. Mixing in the Mediterranean outflow. *Deep-Sea Res.,* **26A,** 535–554.

Baringer, M. O., and J. F. Price, 1997: Mixing and spreading of the Mediterranean outflow. *J. Phys. Oceanogr.,* **27,** 1654–1677.

Bracco, A., and J. Pedlosky, 2003: Vortex generation by topography in locally unstable baroclinic flows. *J. Phys. Oceanogr.,* **33,** 207–219.

Brink, K. H., 1997: Deep-sea forcing and exchange processes. *The Sea,* K. H. Brink and A. R. Robinson, Eds., The Global Coastal Ocean: Processes and Methods, Vol. 10, John Wiley and Sons, 151–167.

Bruce, J. G., 1995: Eddies southwest of Denmark Strait. *Deep-Sea Res. I,* **42,** 13–29.

Bryden, H. L., and H. M. Stommel, 1984: Limiting processes that determine basic features of the circulation in the Mediterranean Sea. *Oceanol. Acta,* **7,** 289–296.

Candela, J., 2001: Mediterranean water and global circulation. *Ocean Circulation and Climate: Observing and Modeling the Global Ocean,* G. Siedler, J. Church, and J. Gould, Eds., Academic Press, 419–430.

Carton, X., L. M. Chérubin, J. Paillet, Y. Morel, A. Serpette, and B. Le Cann, 2002: Meddy coupling with a deep cyclone in the Gulf of Cadiz. *J. Mar. Syst.,* **32,** 13–42.

Chérubin, L. M., N. Serra, and I. Ambar, 2003: Low-frequency variability of the Mediterranean undercurrent downstream of Portimão Canyon. *J. Geophys. Res.,* **108,** 3058, doi:10.1029/2001JC001229.

Criado-Aldeanueva, F., J. García-Lafuente, J. M. Vargas, J. Del Río, A. Vásquez, A. Reul, and A. Sánchez, 2006: Distribution and circulation of water masses in the Gulf of Cadiz from in situ observations. *Deep-Sea Res. II,* **53,** 1144–1160.

Csanady, G. T., 1978: The arrested topographic wave. *J. Phys. Oceanogr.,* **8,** 47–62.

Etling, D., F. Gelhardt, U. Schrader, F. Brennecke, G. Kuhn, G. Chabert d' Hieres, and H. Didelle, 2000: Experiments with density currents on a sloping bottom in a rotating fluid. *Dyn. Atmos. Oceans,* **31,** 139–164.

Gebbie, G., 2004: Subduction in an eddy-resolving state estimate of the northeast Atlantic Ocean. Ph.D. thesis, Massachusetts Institute of Technology, 201 pp.

Gnanadesikan, A., and Coauthors, 2006: GFDL's CM2 global coupled climate models. Part II: The baseline ocean simulation. *J. Climate,* **19,** 675–697.

Gould, W. J., 1985: Physical oceanography of the Azores Front. *Prog. Oceanogr.,* **14,** 167–190.

Hallberg, R., 1997: Stable split time stepping schemes for large-scale ocean modeling. *J. Comput. Phys.,* **135,** 54–65.

Høyer, J. L., D. Quadfasel, and O. B. Anderson, 2002: Deep ocean currents detected with satellite altimetry. *Can. J. Remote Sens.,* **28,** 556–566.

Jia, Y., 2000: Formation of an Azores Current due to Mediterranean overflow in a modeling study of the North Atlantic. *J. Phys. Oceanogr.,* **30,** 2342–2358.

Jiang, L., and R. W. Garwood, 1996: Three-dimensional simulations of overflows on continental slopes. *J. Phys. Oceanogr.,* **26,** 1214–1233.

Käse, R. H., and W. Krauss, 1996: The Gulf Stream, the North Atlantic Current, and the origin of the Azores Current. *The Warmwater Sphere of the North Atlantic Ocean,* W. Krauss, Ed., Gebrüder Borntraeger, 291–337.

——, A. Biastoch, and D. B. Stammer, 2001: On the mid-depth circulation in the Labrador and Irminger Seas. *Geophys. Res. Lett.,* **28,** 3433–3436.

Kida, S., 2006: Overflows and upper ocean interaction—A mechanism for the Azores Current. Ph.D. thesis, MIT/WHOI Joint Program, 144 pp.

Kielmann, J., and R. H. Käse, 1987: Numerical modeling of meander and eddy formation in the Azores Current frontal zone. *J. Phys. Oceanogr.,* **17,** 529–541.

Klein, B., and G. Siedler, 1989: On the origin of the Azores Current. *J. Geophys. Res.,* **94,** 6159–6168.

Lane-Serff, G. F., and P. G. Baines, 1998: Eddy formation by dense flows on slopes in a rotating fluid. *J. Fluid Mech.,* **363,** 229–252.

Lavender, K. L., W. B. Owens, and R. E. Davis, 2005: The mid-depth circulation of the subpolar North Atlantic Ocean as measured by subsurface floats. *Deep-Sea Res. I,* **52,** 767–785.

Legg, S., R. W. Hallberg, and J. B. Girton, 2006: Comparison of entrainment in overflows simulated by z-coordinate, isopycnal and non-hydrostatic models. *Ocean Modell.,* **11,** 69–97.

Le Traon, P. Y., and P. De Mey, 1994: The eddy field associated with the Azores Front east of the Mid-Atlantic ridge as observed by the Geosat altimeter. *J. Geophys. Res.,* **99,** 9907–9924.

Levitus, S., 1982: *Climatological Atlas of the World Ocean.* NOAA Prof. Paper 13, 173 pp. and 17 microfiche.

Machín, F., J. L. Pelegrí, A. Marrero-Díaz, I. Laiz, and A. W. Ratsimandresey, 2006: Near-surface circulation in the southern Gulf of Cádiz. *Deep-Sea Res. II,* **53,** 1161–1181.

Mauritzen, C., Y. Morel, and J. Paillet, 2001: On the influence of Mediterranean Water on the Central Waters of the North Atlantic Ocean. *Deep-Sea Res. I,* **48,** 347–381.

Maximenko, N. A., and P. P. Niiler, 2005: Hybrid decade-mean global sea level with mesoscale resolution. *Recent Advances in Marine Science and Technology, 2004,* N. Saxena, Ed., PACON International, 55–59.

New, A. L., Y. Jia, M. Coulibaly, and J. Dengg, 2001: On the role of the Azores Current in the ventilation of the North Atlantic Ocean. *Prog. Oceanogr.,* **48,** 163–194.

Ochoa, J., and N. A. Bray, 1991: Water mass exchange in the Gulf of Cadiz. *Deep-Sea Res.,* **38** (Suppl.), S465–S503.

Onken, R., 1993: The Azores Countercurrent. *J. Phys. Oceanogr.,* **23,** 1638–1646.

Özgökmen, T. M., E. P. Chassignet, and C. G. H. Rooth, 2001: On the connection between the Mediterranean outflow and the Azores Current. *J. Phys. Oceanogr.,* **31,** 461–480.

——, W. E. Johns, H. Peters, and S. Matt, 2003: Turbulent mixing in the Red Sea outflow plume from a high-resolution nonhydrostatic model. *J. Phys. Oceanogr.,* **33,** 1846–1869.

Paillet, J., and H. Mercier, 1997: An inverse model of the eastern North Atlantic general circulation and thermocline ventilation. *Deep-Sea Res. I,* **44,** 1293–1328.

Paiva, A. M., E. P. Chassignet, and A. J. Mariano, 2000: Numerical simulations of the North Atlantic subtropical gyre: Sensitivity to boundary conditions and horizontal resolution. *Dyn. Atmos. Oceans,* **32,** 209–238.

Pedlosky, J., 1974: Longshore currents, upwelling and bottom topography. *J. Phys. Oceanogr.,* **4,** 214–226.

——, 1987: *Geophysical Fluid Dynamics*. 2nd ed. Springer-Verlag, 710 pp.

Peliz, A., J. Dubert, P. Marchesiello, and A. Teles-Machado, 2007: Surface circulation in the Gulf of Cadiz: Model and mean flow structure. *J. Geophys. Res.,* **112,** C11015, doi:10.1029/2007JC004159.

Plumb, R. A., 1986: Three-dimensional propagation of transient quasi-geostrophic eddies and its relationship with the eddy forcing of the time–mean flow. *J. Atmos. Sci.,* **43,** 1657–1678.

Price, J. F., and M. O. Baringer, 1994: Outflows and deep water production by marginal seas. *Prog. Oceanogr.,* **33,** 161–200.

——, and J. Yang, 1998: Marginal sea overflows for climate simulations. *Ocean Modeling and Parameterizations,* E. P. Chassignet and J. Verron, Eds., Kluwer Academic, 155–170.

——, and Coauthors, 1993: Mediterranean outflow mixing dynamics. *Science,* **259,** 1277–1282.

Rhines, P. B., and W. R. Holland, 1979: A theoretical discussion of eddy-driven mean flows. *Dyn. Atmos. Oceans,* **3,** 289–325.

Rudnick, D. L., and J. R. Luyten, 1996: Intensive surveys of the Azores Front. 1. Tracers and dynamics. *J. Geophys. Res.,* **101,** 923–940.

Smith, P. C., 1975: A streamtube model for bottom boundary currents in the ocean. *Deep-Sea Res.,* **22,** 853–873.

Smith, W. H. F., and D. T. Sandwell, 1997: Global seafloor topography from satellite altimetry and ship depth soundings. *Science,* **277,** 1957–1962.

Spall, M. A., 2000: Buoyancy-forced circulations around islands and ridges. *J. Mar. Res.,* **58,** 957–982.

——, and J. F. Price, 1998: Mesoscale variability in Denmark Strait: The PV outflow hypothesis. *J. Phys. Oceanogr.,* **28,** 1598–1623.

Stramma, L., 1984: Geostrophic transport in the warm water sphere of the eastern subtropical North Atlantic. *J. Mar. Res.,* **42,** 537–558.

Veronis, G. T., 1966: Wind-driven ocean circulation—Part II. Numerical solutions of the nonlinear problem. *Deep-Sea Res.,* **13,** 31–56.

Warren, B. A., 1980: Deep circulation of the world ocean. *Evolution of Physical Oceanography: Scientific Surveys in Honor of Henry Stommel,* B. A. Warren and C. Wunsch, Eds., MIT Press, 6–41.

Whitehead, J. A., A. Leetma, and R. A. Knox, 1974: Rotating hydraulics of strait and sill flows. *Geophys. Fluid Dyn.,* **6,** 101–125.

——, M. E. Stern, G. R. Flierl, and B. A. Klinger, 1990: Experimental observations of baroclinic eddies on a sloping bottom. *J. Geophys. Res.,* **95,** 9585–9610.